3884 *Chem. Mater.* **2010,** *22,* 3884–3899
DOI:10.1021/cm903772n

CHEMISTRY OF
MATERIALS
Article

Si−Ge-based Oxynitrides: From Molecules to Solids

C. Weng, J. Kouvetakis, and A. V. G. Chizmeshya*

Department of Chemistry and Biochemistry, Arizona State University, Tempe, Arizona 85287-1604

Received December 15, 2009. Revised Manuscript Received April 8, 2010

Density functional theory simulations are used to predict ground state crystal structures, electronic properties, and thermodynamic stability of a new class of $Si_{1-x}Ge_xN_2O$ oxynitride materials with potential applications as tunable dielectrics. Thermochemical simulations are also used to explore their possible synthetic routes via reactions of ammonia with (a) mixtures of $(SiH_3)_2O$ and $(GeH_3)_2O$, and (b) a single-source heteronuclear analogue SiH_3OGeH_3. To obtain quantitative values for the above reaction energies we implement a consistent computational methodology to simulate the structural and thermochemical properties of both molecular *and solid state* reactants and products at finite-temperature. In the case of the well-known $(SiH_3)_2O$ and $(GeH_3)_2O$ compounds our calculated molecular structures and vibrational spectra are in excellent agreement with experiment. The hypothetical SiH_3OGeH_3 molecule is predicted to possess an intermediate molecular structure and energy, with stability differences on the order of 1−2 kcal/mol between SiH_3OGeH_3 and mixtures of $(SiH_3)_2O/(GeH_3)_2O$. For the solids we predict two new ordered structures: (i) an α-$SiGeN_2O$ phase composed of a uniform distribution of SiN_3O and GeN_3O tetrahedra, and (ii) a "pseudo-lamellar" form β-$SiGeN_2O$ in which the SiN_3O and GeN_3O units occupy alternating layers. The structural, electronic, and thermoelastic properties of the latter are then systematically compared to those of Si_2N_2O and Ge_2N_2O. Here again, small energy differences comparable to those in the molecular case are found between the $SiGeN_2O$ polytypes and their Si_2N_2O/Ge_2N_2O analogues. The enthalpy of formation of α-$SiGeN_2O$, β-$SiGeN_2O$, and a random $SiGeN_2O$ alloy are predicted to be comparable, indicating that mixing entropy should favor the disordered solid at high temperatures. Collectively, a remarkable consistency is found for the bond-lengths and bond-angles across molecular and solid-state forms. From an experimental perspective, the recent development of industrial scale synthesis for $(SiH_3)_2O$ suggests that the Ge-based analogues proposed here might be accessed using similar approaches, opening the door to new chemically compatible Si−Ge−O−N high-*k* gate materials for high mobility Si−Ge based applications.

1. Introduction

Materials based on compositions Si−Ge−O−N continue to attract considerable attention as functional components in a variety of high-technology applications in the areas of microelectronic and optoelectronic, including telecommunication. Recently quarternary hybrids of Si−Ge oxynitrides with formula "MO_2-M'_3N_4" (M,M′ = Si, Ge) and compositions such as $Si_{1-x}Ge_xO_{2(1-y)}N_{1.33y}$ have been proposed as variable index of refraction (1.4−2.1) materials for niche waveguide applications in planar lightwave circuits.[1,2] Films of this material are typically grown on Si substrates using traditional methods based on plasma-assisted multisource reactions (e.g., SiH_4 and NH_3 as the source of Si and N) which invariably lead to the incorporation of N−H impurities, with corresponding hydrogen levels up to 20%. This approach also produces local variations in composition and bonding throughout the films which exacerbate the thermal mismatch with the substrate causing birefringence in waveguides. These impurities also lead to processing difficulties (film delamination/cracking) and unacceptable optical losses because of vibrational overtones of the N−H resonance near the critical 1.55 μm communication band, ultimately vitiating widespread application in photonic devices.

In contrast, the closely related Si_xN_yO ternaries have become ubiquitous in the area of silicon microelectronics because of their utility as both dielectric and spacer components. As high-*k* gate dielectrics, silicon oxynitrides offer significant advantages over their pure oxide ($y = 0$) counterparts, including fewer interface defects and the ability to act as barriers to conventional boron, phosphorus, and arsenic dopants diffusing from the polycrystalline Si gate into the substrate.[3] In this context the stoichiometric Si_2N_2O derivative has a higher dielectric constant, and it is more likely to form a chemically robust, ordered structure adjacent to the Si interface.[4−6] Accordingly, this material could be used to further mitigate current leakage and suppress dopant penetration while maintaining high gate capacitance over the reduced length scales anticipated in modern devices. Recently we demonstrated the fabrication of Si_2N_2O films via

---

*Corresponding author.

(1) Akwani, I. A.; Bellman, R. A.; Grandi, T. P.; Sachenik, P. A. Germanium silicon oxynitride films with high refractive index for planar waveguides. PCT Int. Appl. (2001), p 25 CODEN: PIXXD2, Patent WO2001034530 A1 2001051.

(2) Osinsky, A. V.; Bellman, R. A.; Akwani, I. A.; Sachenik, P. A.; Logunov, S. L.; McCamy, J. W. *Appl. Phys. Lett.* **2002**, *81*, 2002.

(3) Ellis, K. A.; Buhrman, R. A. *Appl. Phys. Lett.* **1999**, *74*, 967.

(4) Xu, Y.-N.; Ching, W. Y. *Phys. Rev. B* **1995**, *51*, 17379.

(5) Tong, Q.; Wang, J.; Li, Z.; Zhou, Y. *J. Eur. Ceram. Soc.* **2007**, *27*, 4767.

(6) Hillert, H.; Jonsson, S.; Sundman, B. *Z. Metallkd.* **1992**, *83*, 648.

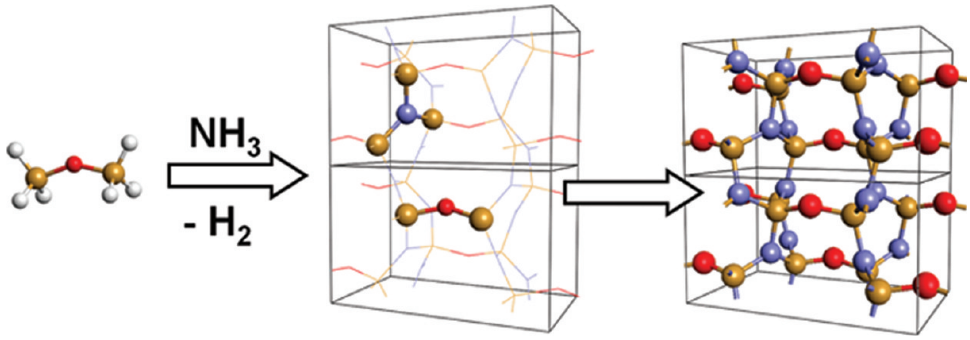

Figure 1. Schematic illustration of the "nano-synthesis" concept showing the assembly of −Si−O−Si− molecular cores (left) to form the Si_2N_2O (right). The central panel highlights the coordination of the oxygen and nitrogen atoms with respect to the silicon sublattice nearest neighbors.

reactions of disiloxane $H_3SiOSiH_3$ and a large excess of NH_3 according to the reaction shown by eq 1.[7]

$$H_3SiOSiH_3(g) + 2NH_3(g) \rightarrow Si_2N_2O(s) + 6H_2(g) \quad (1)$$

In this "nano-synthesis" approach the molecular Si−O−Si cores of $(SiH_3)_2O$ deliver both the compositional and bonding configuration at the nanoscale required to form the desired solid-state material, as illustrated in Figure 1. Accordingly, the Si_2N_2O phase can be viewed as a periodic assembly of Si−O−Si building blocks linked together at the Si sites by trigonal nitrogen centers (Figure 1). In contrast to the formation of the above $Si_{1-x}Ge_xO_{2(1-y)}N_{1.33y}$ and Si_xN_yO materials, obtained from reactions of NH_3 with SiH_4[8,9] (or chlorosilane derivatives), our $H_3SiOSiH_3$-based process guarantees control of composition *and structure* at the nanoscale. Perhaps more importantly, the reproducibility needed to achieve large-scale production is ensured since precise control of the NH_3 activity is not required in the reaction medium. This is particularly attractive from a processing perspective since $(SiH_3)_2O$ is the limiting reagent while nitrogen (derived from NH_3) is only incorporated to the degree required to achieve the Si_2N_2O stoichiometry and structure. In contrast, the use of multisource reactions (e.g., SiH_4, NH_3, etc.) invariably produces extraneous bonding arrangements which promote the incorporation of deleterious N−H bonds which, as noted above, can ultimately degrade the structural, dielectric, and optical performance of the materials.

Oxynitrides in the Si−Ge−O−N family are also expected to play an important role in the next generation of high speed transistors containing elemental Ge channels, which possess a higher mobility than their Si-based counterparts. This necessitates the fabrication of compatible gate dielectric analogues grown directly on the surface of the transistor channel—a role which has so far been fulfilled by GeO_2 and HfO_2. However, because of hydrolytic and thermodynamic instability, the classical GeO_2 phase and related non-stoichiometric derivatives complicate subsequent complementary metal oxide semiconductor (CMOS) processing. For this reason hafnium oxide based dielectrics were initially explored but they were also found to be problematic because they reacted with Ge to form undesirable intermediates which interfere with the function of the device. The most promising, chemically compatible alternatives for this purpose are Ge_xN_yO systems[10,11] (and possibly Ge_2N_2O, the Ge analogue of Si_2N_2O) which have recently attracted increasing interest. In a more general context the pseudobinary $Si_{1-x}Ge_xN_2O$ compounds may be of significant technological interest, particularly from the point of view of applications in the emerging area of SiGe- and Ge-based microelectronics. From a molecular perspective a possible route to stoichiometric or non-stoichiometric Ge oxynitides could be developed in analogy with that depicted in eq 1 using reactions involving $(GeH_3)_2O$ in place of the $(SiH_3)_2O$:

$$GeH_3OGeH_3(g) + 2NH_3(g) \rightarrow Ge_2N_2O(s) + 6H_2(g) \quad (2)$$

This also opens the door to the design and synthesis of novel pseudobinary compounds that are intermediate between the Si_2N_2O and Ge_2N_2O phases such as $(Si,Ge)_2N_2O$ or solid solutions with compositions $Si_{1-x}Ge_xN_2O$. While reaction 1 has been previously implemented using low pressure chemical vapor deposition (CVD) in our laboratories there are no reports (to our knowledge) describing the use of the analogous reaction pathway 2 to produce Ge_2N_2O films, despite the promise of this method to yield high-purity stoichiometric material, that might be useful for the fabrication of Ge-based gate dielectrics. In this context, another plausible route to the formation of oxynitride dielectrics containing both Si and Ge, such as the stoichiometric hybrid $SiGeN_2O$, could involve reactions analogous to 1 and 2 such as:

$$SiH_3OGeH_3(g) + 2NH_3(g) \rightarrow SiGeN_2O(s) + 6H_2(g) \quad (3)$$

where SiH_3OGeH_3 represents a new asymmetrical analogue of $(SiH_3)_2O$ and $(GeH_3)_2O$.

---

(7) Torrison, L.; Tolle, J.; Kouvetakis, J.; Dey, S. K.; Gu, D.; Tsong, I. S. T.; Crozier, P. A. *Mater. Sci. Eng., B* **2003**, *97*, 54.

(8) Gusev, E. P.; Lu, H.-C.; Garfunkel, E. L.; Gustafsson, T.; Green, M. L. *IBM J. Res. Devel.* **1999**, *43*(3), 265.

(9) Green, M. L.; Gusev, E. P.; Degraeve, R.; Garfunkel, E. L. *J. Appl. Phys.* **2001**, *90*(5), 2057.

(10) Chui, C. O.; Ito, F.; Saraswat, K. C. *IEEE Electron Device Lett.* **2004**, *25*(9), 613.

(11) Sugawara, T.; Sreenivasan, R.; McIntyre, P. C. *J. Vac. Sci. Technol. B.* **2006**, *24*, 2449.

Although a considerable theoretical and experimental knowledge-base exists for the reactants $(SiH_3)_2O^{12-16}$ and $(GeH_3)_2O^{17-20}$ and products $Si_2N_2O^{4,21-25}$ and $Ge_2N_2O^{24-26}$ in eq 1 and 2, the corresponding properties of the SiH_3O-GeH_3 species and solid $SiGeN_2O$ phases in reaction eq 3 are completely unknown. Accordingly the relationship between the properties of the asymmetrical analogues and the average behavior of the corresponding Si- and Ge- based molecules and solids is of considerable interest. Our primary objective in the present work is therefore to explore, from a theoretical perspective, the feasibility of forming the $SiGeN_2O$ hybrids using the molecular approaches described above. To elucidate the thermodynamics of these reactions we first study the properties of the $(SiH_3)_2O$ and $(GeH_3)_2O$ reactants in detail. The outcomes from these calculations are validated by comparing the predicted formation enthalpies and vibrational spectra with their experimental counterparts. On the basis of the excellent agreement found, we then predict the properties of the heteronuclear analogue SiH_3OGeH_3 proposed as a single source precursor for the direct synthesis of $SiGeN_2O$. We show that the latter molecule possesses an atomic structure and energetic stability intermediate to that of the symmetrical Si and Ge molecular species. Next, we consider the properties of the solid products Si_2N_2O, Ge_2N_2O and $SiGeN_2O$. Here we propose the existence of two mixed Si−Ge hybrids α-$SiGeN_2O$ and β-$SiGeN_2O$ possessing homogeneous and anisotropic Si/Ge spatial distributions, respectively, and compare their electronic, thermodynamic, and elastic properties with those of the pure Si and Ge end members. Finally, the calculated thermochemical properties of the gas and solid phase reactants and products are combined to produce quantitative estimates of the reaction free energies. By systematically studying the energetics of intermediate nanoscale building blocks possessing the same local bonding structure as the target solids we propose several plausible reaction mechanisms to produce the α-$SiGeN_2O$ and β-$SiGeN_2O$ phases.

2. Computational Details and Approach

Quantitative estimates of thermochemical reaction processes between gases and solids, such as those described by eqs 1−3, requires a systematic treatment of both the isolated gas phase molecules and the periodic solids at a fundamental level. For molecular systems state-of-the-art packages such as Gaussian03[27] provide an efficient means of computing the ground state molecular, electronic, and vibrational structure. This information is then used to generate estimates of various thermodynamic functions such as the enthalpy, entropy, and free-energy at desired temperatures and pressures. It should be noted that, for free molecules, the rotational and translational contributions to the thermodynamic functions are also explicitly included. The consistent treatment of reaction thermodynamics involving purely gas phase reactants and products is therefore completely accessible within this computational framework.

By contrast, the systematic calculation of thermochemistry in solids is significantly more challenging. While the absence of free translational and rotational degrees of freedom implies that thermal corrections to the electronic energy are dominated by vibrational contributions these necessitate the calculation of the harmonic phonon spectrum of the lattice $\{\omega_{n,\mathbf{k}}\}$, where n and $\mathbf{k}$ label the phonon mode and the wave vector, respectively, which is computationally intensive. Various thermodynamic functions are then typically obtained by invoking the quasi-harmonic approximation,[28] which states that the thermal contribution to the energy for any structural configuration $\{\mathbf{R}\}$ (unit cell parameters and corresponding internal atomic coordinates) is given by that of the corresponding harmonic system. In principle, the equilibrium structural parameters at a given pressure P and temperature T are those that minimize the Gibbs free energy on the adiabatic electronic surface according to

$$G(T,P) = \min_{\{\mathbf{R}\}}[E(\mathbf{R}) + F_{VIB}(\mathbf{R};T) + PV(\mathbf{R})] \tag{4}$$

where E is the electronic energy evaluated using the parameters $\{\mathbf{R}\}$ and the "constrained" vibrational free-energy function is given by

$$F_{VIB}(\mathbf{R};T) = \sum_{n,\mathbf{k}} \left[\frac{1}{2}\hbar\omega_{n,\mathbf{k}} + k_B T \ln(1 - e^{-\hbar\omega_{n,\mathbf{k}}/k_B T})\right] \tag{5}$$

In the above formula the phonon frequencies depend implicitly on all the crystalline structural degrees of freedom $\{\mathbf{R}\}$. A more common approach encountered in the literature is to minimize the free energy of a given solid phase at a given temperature with respect to volume only, and not the full set of structural parameters $\{\mathbf{R}\}$. In the present work, we adopt this simplified approach (see below) which assumes that the vibrational free energy is isotropic with respect to all structural parameters $\{\mathbf{R}\}$.

To unify the treatment of the gases and solids appearing in reactions eqs 1−3 we adopt a combined approach involving the molecular thermochemistry methodology as implemented in the Gaussian03 code, and crystal thermochemistry derived from

---

(12) Al Derzi, A. R.; Gregusova, A.; Runge, K.; Bartlett, R. J. *Int. J. Quantum Chem.* **2008**, *108*, 2088–2096.
(13) Phadungsukanan, W.; Shekar, S.; Shirley, R.; Sander, M.; West, R. H.; Kraft, M. *J. Phys. Chem. A* **2009**, *113*, 9041–9049.
(14) Almenningen, A.; Bastiansen, O.; Ewing, V.; Hedbeg, K.; Trettebreg, M. *Acta Chem. Scand.* **1963**, *17*, 2455.
(15) Torrison, L.; Tolle, J.; Smith, D. J.; Poweleit, C.; Menendez, J.; Mitan, M. M.; Alford, T. L.; Kouvetakis, J. *J. Appl. Phys.* **2002**, *92*(12), 7475.
(16) Tice, J. B.; Weng, C.; Tolle, J.; D'Costa, V. R.; Singh, R.; Menendez, J.; Kouvetakis, J.; Chizmeshya, A. V. G. *Dalton Trans.* **2009**, *34*, 6773–6782.
(17) Basch, H. *Inorg, Chim, Acta* **1996**, *252*, 265–279.
(18) Jensen, J. O. *Spectrochim, Acta, Part A* **2004**, *60*, 2581–2585.
(19) Livant, P.; Northcott, J.; Webb, T. R. *J. Organomet. Chem.* **2001**, *620*, 133–138.
(20) Glidwell, C.; Rankin, D. W. J.; Robiette, A. G.; Sheldrick, G. M.; Beagley, B.; Cradock, S. *J. Chem. Soc. A: Inorg., Phys., Theor.* **1970**, *2*, 315–317.
(21) Kroll, P.; Milko, M. *Z. Anorg. Allg. Chem.* **2003**, *629*, 1737.
(22) Haines, J.; Santoro, M. *Phys. Rev. B* **2008**, *77*, 144206.
(23) Srinivasa, S. R.; Cartz, L.; Jorgensen, J. D.; Worlton, T. G.; Beyerlein, R. A.; Billy, M. *J. Appl. Crystallogr.* **1977**, *10*, 167–171.
(24) Ching, W. Y.; Ren, S.-Y. *Phys. Rev. B* **1981**, *24*, 5788.
(25) Ivanovskii, A. L.; Medvedeva, N. I.; Kontsevoi, O. Y.; Shveikin, G. P. *Phys. Status Solidi* **2000**, *221*, 647.
(26) Srinivasa, S. R.; Cartz, L.; Jorgensen, J. D.; Labbe, J. C. *J. Appl. Crystallogr.* **1979**, *12*, 511.
(27) Frisch, M. J. et al. *Gaussian 03*, Revision B.04; Gaussian Inc: Wallingford, CT, 2003.
(28) Wallace, D.C. *Thermodynamics of Crystals*; John Wiley & Sons, Inc.: New York, 1972.

energies, structures, and vibrational properties calculated using the Vienna Ab-initio Simulation Package (VASP).[29] While the former code uses Gaussian functions (basis sets) to mathematically represent molecular electronic functions, the latter employs plane-waves in the periodic context. Nevertheless, using appropriate precautions the VASP code can also be used to treat molecules, for example, by placing them on a widely spaced periodic grid to suppress artificial interactions. Using a common density functional theory (DFT) framework as a "bridge" between these two methodologies we establish the computational conditions necessary for either approach to yield the same ground state molecular structures. Under these conditions the thermal corrections to the electronic energy obtained from the Gaussian03 code become transferable. The VASP code is then used to accurately compute a consistent set of electronic energies for all gas and solid phase reactants and products. Approximate thermal corrections are then applied to these energies to generate quantitative predictions of the reaction free energies corresponding to eqs 1−3. This strategy is crucial in the present work because of the delicate energy balances exhibited by the Si−Ge−N−O systems, as we demonstrate a posteriori below.

To study the thermochemistry of the molecules we employ three model chemistries: (i) the hybrid B3LYP[30] DFT functional, (ii) the CBS-QB3[31] compound method, and (iii) the GGA-PW91[32] density functional. Method (i) is a popular choice for the efficient and quantitative description of molecular structure and vibrational properties, while approach (ii) combines various model chemistries and scaling properties to achieve a high predictive capability for thermodynamic properties. The PW91-GGA DFT treatment in (iii) has been demonstrated to provide reliable binding energies and consistent structural predictions for both molecule and solids. Furthermore, it is available in both the Gaussian03 molecular code and the solid state VASP code. All Gaussian03 DFT calculations based on the B3LYP and PW91-GGA functionals were carried out using a 6-311N++G(3df,3pd) basis set, "tight" convergence criteria for the structural optimizations and no symmetry constraints. The dynamic stability of the optimized equilibrium molecular structures was confirmed by carrying out vibrational calculations to verify that all normal modes have positive definite frequencies. The vibrational data from these calculations was then used to generate the thermochemistry output. For the CBS-QB3 calculations standard internal default settings were employed. The treatment of the gas phase species using the VASP code involved placing each molecule at the center of a slightly orthorhombic supercell with edge lengths ~20 Å. This length scale ensures a negligible interaction between the contents of adjacent cells. We note that isolated atoms/molecules treated in a completely symmetric cell have a tendency to converge to a false minimum; thus a slightly distorted cell was used to break the symmetry in the periodic setting. In all cases the PAW-GGA methodology was employed with an 800 eV energy cutoff for the plane-wave expansion and a single *k*-point at Γ. All calculations involving Ge atoms employed pseudopotentials which explicitly include the 3d electrons.[33]

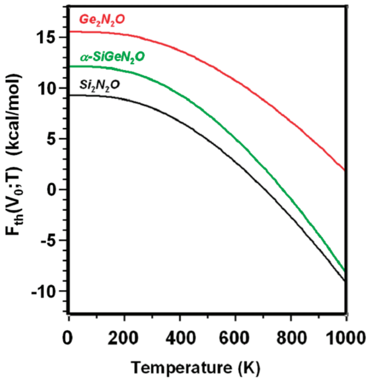

Figure 2. Temperature dependence of the vibrational free energy (per formula unit) obtained from the quasi-harmonic approximation.

The spectrum of normal mode vibrational frequencies needed to simulate the thermochemistry of the various oxynitrides, was obtained using the *fropho* code[34] in which a finite number of special "frozen phonon" displacements is applied to the ground state equilibrium structure to generate the force constant (and mass-weighted dynamical) matrix. For the oxynitride solids considered here less than a dozen such displacements are typically needed to generate all of the required matrix elements. A 2 × 2 × 2 orthorhombic supercell representation containing 160 atoms was found to be sufficient in all cases to convergence of the matrix elements with respect to near-neighbor contributions. Exceedingly high convergence tolerances were required to generate the stress-free and zero-atomic force equilibrium starting structures needed for the dynamical calculations. Typically we employed a value -1×10^{-8} for the structural criterion EDIFFG, and increased the augmentation grids in the FFT part of the code. To determine the free-energy minimum for each system at 300 K, the constrained free-energy function in eq 5 was added to the *E*(*V*) curve that was generated using about 10 equally spaced volumes around equilibrium, and then fitted to a third order Birch−Murnaghan equation of state.[35] Typical free-energy functions for the Si_2N_2O, Ge_2N_2O, and α-$SiGeN_2O$ compound, evaluated at the corresponding equilibrium volume for each system, are shown in Figure 2. The plot indicates that the free energies generally decrease with increasing temperature. The green curve represents the temperature dependence of the free energy for α-$SiGeN_2O$. Note the departure of the alloy free energy from the average behavior of the pure Si- and Ge- end members indicating a tendency toward increased relative stability at high temperatures. Further details concerning the properties of hypothetical solid phases will be provided below.

3. Molecular Properties of Gas Phase Reactants and Products

3.1. Structural Results. The calculated ground state structures for the gaseous $(SiH_3)_2O$, $(GeH_3)_2O$, SiH_3OGeH_3, NH_3, and H_2, are listed in Table 1 which compares the outcome of the three computational approaches (PW91-GGA, B3LYP, and CBS-QB3) with one another, as well as with experiment (where available). Using all methods listed the Si−O and Ge−O bond lengths and Si−O−Si and Ge−O−Ge bond angles in the $(SiH_3)_2O$ and $(GeH_3)_2O$ closely match those determined using gas phase electron diffraction of these

---

(29) Kresse, G.; Furthmuller, J. *Comput. Mater. Sci.* **1996**, *6*, 15. Kresse, G.; Hafner *J. Phys. Rev. B* **1993**, *47*, 558. Kresse, G.; Furthmuller, J. *J. Phys. Rev. B* **1996**, *54*, 11.

(30) Stephens, P. J.; Devlin, F. J.; Chablowski, C. F.; Frisch, M. *J. Phys. Chem.* **1994**, *98*, 11623, and refs therein.

(31) Montgomery, J. A., Jr.; Frisch, M. J.; Ochterski, J. W.; Petersson, G. A. *J. Chem. Phys.* **1999**, *110*, 2822.

(32) Perdew, J. P.; Wang, Y. *Phys. Rev. B* **1986**, *33*, 8800.

(33) Kresse, G.; Hafner., J. *J. Phys.: Condens. Matter* **1994**, *6*, 8245.

(34) Togo, A.; Oba, F.; Tanaka, I. *Phys. Rev. B* **2008**, *78*, 134106.

(35) Birch, F. J. *Geophys. Res.* **1987**, *83*, 1257.

Table 1. Summary of Thermochemical Data Obtained from Simulation for All Gas and Solid Phase Reactants and Products Involved in Reactions 1−3,[a,b]

system	methodology	b_{MO}	b_{MH}	θ_{MOM}	θ_{HMH}	E_0	E_A	$\Delta G(300K)$
$(SiH_3)_2O$	VASP (PW91)	1 645	1.484	143 1	110.0	−1.47037	−1.11377	
	GO3 (PW91)	1.652	1.487	142.5	110.3	−657.86876	−1.08942	0.02726
	GO3 (B3LYP)	1.638	1.478	150.7	109.8	−657 99054	−1.09711	0.02438
	GO3 (CBS-QB3)	1.638	1.479	154.9	109.8	−656.91038	−1.06124	
	Experiment[14]	***1.634***		***144.1°***				
$(GeH_3)_2O$	VASP (PW91)	1.794	1.536	124.6	110.9	−1.30988	−0.96092	
	GO3 (PW91)	1.797	1.539	124.9	110.5	−4233.08713	−0.95507	0.01803
	GO3 (B3LYP)	1.784	1.536	129.8	110.3	−4232.91385	−0.95002	0.01943
	GO3 (CBS-QB3)	1.789	1.536	132.8	110.4	−4230.17512	−092823	
	Experiment[20]	***1.766***	***1.531***	***126.5°***	***106.4***			
$(SiH_3)O(GeH_3)$	VASP (PW91)	1.647,1.798	1.493, 1.533	131.0	110.1,110.8	−1.39034	−1.03756	
	GO3 (PW91)	1.651, 1.799	1.497, 1.538	131.5	108.8, 109.1	−2445.47830	−1.02260	
	GO3 (B3LYP)	1.637, 1.786	1.481, 1.533	137 4	106.5, 111.5	−244545258	−1.02395	0.02254
	GO3 (CBS-QB3)	1.638,1.790	1.481, 1.534	140.6	111.1,111.8	−2443.54337	−0.99535	
NH_3	VASP (PW91)		1.022		106.6	−0.72023	−0.48571	
	GO3 (PW91)		1.021		106.4	−56.55882	−0.52223	0.01541
	GO3 (B3LYP)		1.013		107.2	−56.58755	−0.58048	0.01614
	GO3 (CBS-QB3)		1.016		106.5	−56.46020	−044021	
	Experiment		***1.012***		***106.7°***		***−0.44143***	
H_2	VASP (PW91)	0.750				−0.24972	−0.16734	
	GO3 (PW91)					−1.17009	−0.16729	−0.00166
	GO3 (B3LYP)					−1.18003	−0 17551	−0.00144
	GO3 (CBS-QB3)	0.744				−1.16608	−0.16645	
	Experiment	***0.741***					***−0.17370***	

[a] M refers to {Si,Ge}, and all energies are quoted in atomic units (Hartree). Bond lengths are given in Angstroms. For the SiH_3OGeH_3 the b_{MO} and b_{MH} columns list both Si- and Ge- related bond lengths, respectively. [b] Note: VASP results above obtained using "hard" PAW-GGA (PW91) potentials for H, O, and Ge. VASP electronic energies reported for molecules is *"energy-without entropy"*. PW91 atomic energies (Hartree): H = −0.50140. N = −54.53239. O = −75.05798. Si = −289.35648. Ge = −2077.03284. B3LYP atomic energies (Hartree): H = −0.50226. N = −54.50029. O = −75.09091. Si = −289.39448. Ge = −2076.92968. VASP atomic pseudo-energies (Hartree): H = −0.04119, N = −0.11095, O = −0.0.1414, Si = −0.02766, Ge = −0.02384. 1 hartree = 627.509 kcal/mol = 2625.50 kJ/mol.

molecules. The molecular cores of $(SiH_3)_2O$ and $(GeH_3)_2O$ also closely reflect the intrinsic bonding arrangements in the corresponding solid state forms (silica and germania) where [$b_{SiO} \sim 1.61$ Å, <SiOSi ∼ 146°] in α-SiO_2 and [$b_{GeO} \sim 1.78$ Å, <GeOGe ∼ 135°] in α-GeO_2. We note that the observed Si−O−Si and Ge−O−Ge bond angles in the molecules are best reproduced by the GGA-DFT method, while the other approaches give deviations as large as 10 degrees. For example, the Ge−O−Ge angle in $(GeH_3)_2O$ obtained at the GGA-DFT level (125°) is very similar to that obtained from gas electron diffraction[20] of 127°, while the Ge−O bond length of 1.77 Å found experimentally is close to our computed value of 1.79 Å. Similar excellent agreement between theory and experiment is found for the structure of the $(SiH_3)_2O$ molecule. For SiH_3OGeH_3 we find that the Si−O−Ge bond angle (131.3°) is predicted to be within 1−2 degrees of the average between the Si−O−Si and Ge−O−Ge bond angles in $(SiH_3)_2O$ and $(GeH_3)_2O$. Similarly, Si−O and Ge−O bond lengths in SiH_3OGeH_3 are nearly identical to those in the homonuclear analogues. The structure of the remaining gas phase species, NH_3 and H_2, are very also well reproduced by all of the methods, with typical deviations in bond lengths and bond angles on the order of < 1%. Collectively, the best comparison with observed structural data for all molecules is obtained from the GGA-DFT method using either the Gaussian03 or the VASP codes, in spite of their manifestly different numerical implementations of the formalism (e.g., Gaussian basis set vs plane-wave expansion).

3.2. Atomization Energies. The equilibrium ground state electronic energies for all molecular species are listed as E_0 for all of the methods employed in Table 1. To enable the direct comparison of relative energies across the different methods we computed the *static* atomization energies E_A for all species, which represent the energy needed to completely dissociate the molecule into its constituent atoms. For each computational scheme listed, the latter are obtained by subtracting the spin-polarized ground state energy of the constituent atoms from E_0. These appear at the bottom of Table 1 for all atoms involved. In general we find that the atomization energies obtained using the compound CBS-QB3 method are in excellent agreement with the available experimental values, with discrepancies of ∼0.7 and 4.3 kcal/mol for H_2 and NH_3, respectively. We note that the latter, however, implicitly include room temperature ($T \sim 298$ K) thermal corrections. For the DFT methods (PW91-GGA and B3LYP) the inclusion of $T = 298$ K free-energy corrections to the static atomization values reduces the discrepancy with experiment from −10% to −6% for NH_3 and from +3.7% to +2.3% for H_2. It should be noted that the largest variation in the calculated atomization energy using various DFT methods employed (0.0368 $H = 1$ eV = 23.06 kcal/mol) is found in the NH_3 molecule. This is a well-known problem, and it has been demonstrated that exceedingly high quality basis sets (e.g., aug-cc-pV5Z), and anharmonic thermodynamic corrections, are required to obtain a reasonable description of the atomization energy and electron affinity in this system.[36] Here we find that the standard 6-311N++G(3df,3pd) basis set as implemented in Gaussian03 does not appear to perform as well as the description afforded by the plane-wave expansion as implemented in the VASP code. Finally, we note that the GGA values obtained for E_A for all molecules is

---

(36) Martin, J. M. L.; Lee, T. J. *Chem. Phys. Lett.* **1996**, *258*, 136.

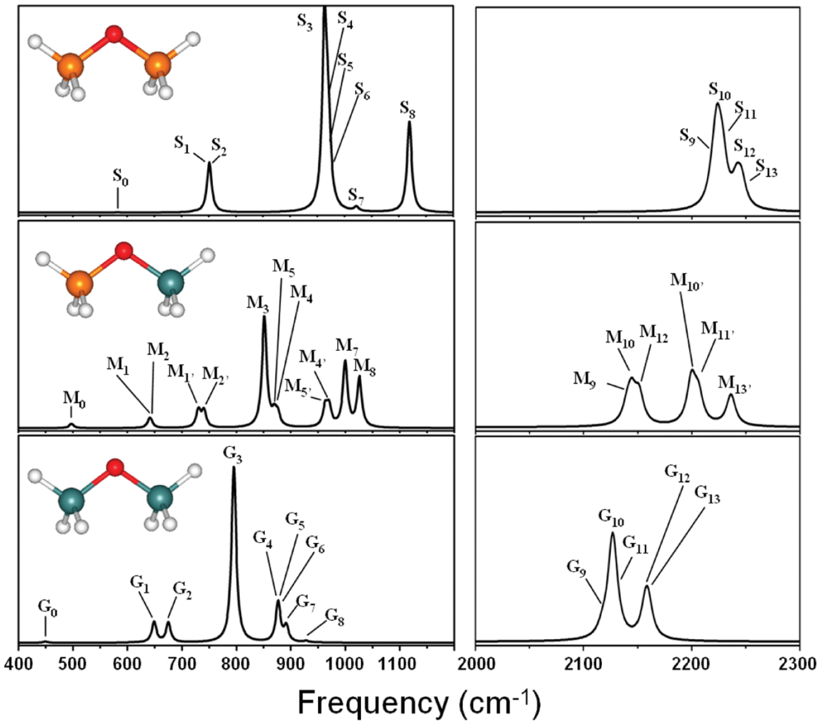

Figure 3. Calculated infrared spectra of the $(SiH_3)_2O$, $(GeH_3)O(SiH_3)$, and $(GeH_3)_2O$ molecules (in order from top to bottom). Left and right panels contain the low- and high-frequency spectra, respectively, and no frequency scale factors have been applied.

Table 2. Frequencies and Mode Assignments for the Infrared Spectra of the $(SiH_3)_2O$, $(GeH_3)O(SiH_3)$, and $(GeH_3)_2O$ Molecules[a]

SiH_3OSiH_3		SiH_3OGeH_3		GeH_3OGeH_3		primary mode assignments
So	582	M_o	498	G_o	450	Si/Ge−O−Si/Ge symmetric stretchmg
		M_1	641	G_1	649	out-of-phase GeH_2 wagging
S_1	751	$M_{1'}$	730			out-of-phase SiH_2 wagging
		M_2	643	G_2	675	out-of-phase GeH_3 wagging
S_2	752	$M_{2'}$	740			out-of-phase SiH_3 wagging
S_3	963	M_3	851	G_3	795	In-phase SiH_3/GeH_3 wagging
		M_4	876	G_4	876	out-of-phase GeH_2 scissors
S_4	967	$M_{4'}$	970			out-of-phase SiH_2 scissors
		M_5	870	G_5	876	In-phase GeH_3 scissors
S_5	970	$M_{5'}$	963			in-phase SiH_3 scissors
S_6	971			G_6	878	in-phase SiH_2/GeH_2 scissors
S_7	1022	M_7	1000	G_7	892	out-of-phase SiH_3/GeH_3 wagging
S_8	1119	M_8	1025	G_8	928	Antisymmetric Si/Ge−O−Si/Ge stretching
S_9	2219	M_9	2140	G_9	2118	out-of-phase swim. SiH_3/GeH_3 stretching
*	2219			*	2120	out-of-phase asymm. SiH_3/GeH_3 stretching
		M_{10}	2144	G_{10}	2127	in-phase asymmetric GeH_2 stretching
S_{10}	2223	$M_{10'}$	2200			in-phase asymmetric SiH_2 stretching
S_{11}	2228	$M_{11'}$	2206	G_{11}	2129	in-phase symmetric SiH_2/GeH_2 stretching
S_{12}	2241	M_{12}	2151	G_{12}	2157	out-of-phase SiH/GeH stretching
S_{13}	2246	$M_{13'}$	2236	G_{13}	2160	in-phase SiH/GeH stretching

[a] The vibrational modes, labeled S_m, M_m, and G_m, correspond to the features shown in Figure 3.

found to be similar using the Gaussian03 and VASP methods, with typical differences on the order of 1−2%.

3.3. Vibrational Spectroscopy. Our prior computational studies have demonstrated that the B3LYP functional, combined with a 6-311N++G(3df,3pd) basis set, provides an excellent quantitative account of the observed infrared spectrum of a range of Si−Ge hydrides.[37−41] Accordingly, we used the same prescription to simulate the infrared spectra of $(SiH_3)_2O$, $(GeH_3)O(SiH_3)$, and $(GeH_3)_2O$. Figure 3 shows plots of the low- and high-frequency range of the spectra, while the corresponding frequencies and mode assignments are listed in Table 2 (we note that the standard frequency scale factors typically used to reconcile theory with experiment have not been applied). All of the assignments

---

(37) Chizmeshya, A. V. G.; Ritter, C. J.; Hu, C.; Tolle, J.; Nieman, R. A.; Tsong, I. S. T.; Kouvetakis, J. *J. Am. Chem. Soc.* **2006**, *128*, 6919.

(38) Ritter, C. J.; Hu, C.; Chizmeshya, A. V. G.; Tolle, J.; Klewer, D.; Tsong, I. S. T.; Kouvetakis, J. *J. Am. Chem. Soc.* **2005**, *127*, 9855.

(39) Tice, J. B.; Chizmeshya, A. V. G.; Roucka, R.; Tolle, J.; Cherry, B. R.; Kouvetakis, J. *J. Am. Chem. Soc.* **2007**, *129*, 7950.

(40) Tice, J. B.; Fang, Y.-Y.; Tolle, J.; Chizmeshya, A.; Kouvetakis, J. *Chem. Mater.* **2008**, *20*, 4374.

(41) Tice, J. B.; Weng, C.; Tolle, J.; D'Costa, V. R.; Singh, R.; Menendez, J.; Kouvetakis, J.; Chizmeshya, A. V. G. *Dalton Trans.* **2009**, *34*, 6773.

shown in Table 2 were made by systematically examining each normal mode displacement pattern in the molecular spectra. According to our calculations, the most intense infrared features in this class of molecules occur in the frequency range from 800 to 1000 cm^{-1}, and arise from in-phase SiH_3/GeH_3 wagging motions. These modes are designated as S_3, M_3, and G_3 in $(SiH_3)_2O$, $(GeH_3)O(SiH_3)$, and $(GeH_3)_2O$, respectively (see Figure 3). The corresponding out-of-phase SiH_3/GeH_3 wags (S_7, M_7, and G_7) are much weaker and typically occur at frequencies ~70−150 cm^{-1} higher than their in-phase counterparts. The weaker intensity features in all three molecules ($S_{1,2}$, $M_{1,2}$, $M_{1',2'}$, and $G_{1,2}$) arise predominantly from out-of-phase, but symmetric, GeH_2/SiH_2 wagging motions. (Note: here the terms "in-phase" and "out-of-phase" refer to vibrational patterns that are synchronous/asynchronous with respect to the oxygen center). In the case of the latter wagging motions we find that the SiH_2 and GeH_2 wags in all molecules occur in a narrow frequency range from ~730−750 cm^{-1} and ~640−670 cm^{-1}, respectively. This can be clearly seen from the close alignment of the (S_1,S_2) features in $(SiH_3)_2O$ and the ($M_{1'}$,$M_{2'}$) in the $(GeH_3)O(SiH_3)$ analogue. A similar close correspondence is observed between the (G_1,G_2) modes of $(GeH_3)_2O$ and the (M_1,M_2) modes in $(GeH_3)O(SiH_3)$. The least intense S_0, M_0, and G_0 features are associated with symmetric (Si,Ge)−O−(Si,Ge) skeletal stretching, and exhibit a systematic downshift in frequency with increasing mass of the terminal Si/Ge atoms, as expected (e.g., the progression of these frequencies is in the order $\nu_{Si-O-Si} > \nu_{Si-O-Ge} > \nu_{Ge-O-Ge}$). We note that the exceedingly weak S_0 mode, predicted to occur ~582 cm^{-1} in the $(SiH_3)_2O$ molecule, is not visible in Figure 3. The most dramatic intensity variation observed among the low-frequency modes in the three molecules is predicted to occur in the antisymmetric (Si,Ge)−O−(Si,Ge) stretching bands S_8, M_8, and G_8 for which the intensities follow the ratio $I(S_8)/I(M_8)/I(G_8) \sim 1.0{:}0.5{:}0.0$. Note that these modes also exhibit downward frequency shifts with increasing mass of the terminal Si/Ge atoms, in complete analogy with their symmetric S_0, M_0, and G_0 counterparts. As to the various H−Si−H and H−Ge−H scissor modes, these are predicted to occur in a narrow frequency range from ~960−970 cm^{-1} and ~870−880 cm^{-1}, respectively. Accordingly, in $(SiH_3)_2O$ these modes (S_4,S_5,S_6) overlap with the high-frequency shoulder of the intense S_3 mode, and are therefore difficult to resolve (see Figure 3).

The high-frequency infrared spectra (2000−2300 cm^{-1}) of $(SiH_3)_2O$, $(GeH_3)O(SiH_3)$, and $(GeH_3)_2O$ are shown in the right panels of Figure 3. These bands are due to symmetric and asymmetric Si−H and Ge−H stretching vibrations of the terminal SiH_3 and GeH_3 groups. The basic shape of these bands in the $(SiH_3)_2O$ and $(GeH_3)_2O$ compounds is typical of Si and Ge hydrides, with the most intense peaks (S_{10} and G_{10}, respectively) being due to the asymmetric stretching modes. In the present case, however, weak *symmetric* stretching vibrations possessing an out-of-phase displacement pattern with respect to the two Si/Ge terminal groups are shifted to lower frequencies (2219 cm^{-1} and 2118 cm^{-1}, respectively) with respect to the pure asymmetric modes. The corresponding asymmetric out-of-phase stretching vibrations occur at the same frequencies but are not IR active (see entries with asterisks in Table 2). Thus both molecules possess six normal modes in the 2000−2300 cm^{-1} range. The high-frequency spectrum of the $(GeH_3)O(SiH_3)$ can be essentially interpreted in terms of the hydrogen bands of $(SiH_3)_2O$ and $(GeH_3)_2O$ (see Table 2). An important distinction is that all six of the high-frequency modes in this molecule involve proton vibrations localized to either the Si or the Ge site, so that the "in-phase"/"out-of-phase" designation is redundant, and can be ignored. Three of these modes (M_9, M_{10}, and M_{12}) correspond closely to their $(GeH_3)_2O$ counterparts both in their character and frequencies (e.g., within ~20 cm^{-1}). Similarly, the modes $M_{10'}$, $M_{11'}$, and $M_{13'}$ correlate in the same fashion with their counterparts in $(SiH_3)_2O$. In the latter case, the splitting between the symmetric and the asymmetric modes in $(SiH_3)_2O$ is more or less preserved in the heteronuclear analogue $(GeH_3)O(SiH_3)$, while the corresponding splitting in the Ge−H modes is significantly reduced.

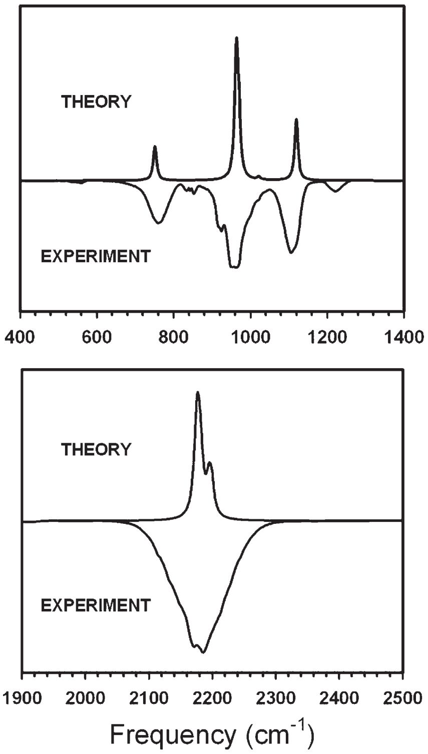

Figure 4. Comparison of the calculated and observed infrared spectrum of $(SiH_3)_2O$. Frequency scale factors of 0.989 and 0.979 have been applied to the low- and high-frequency theoretical spectra as described in the text.

Our calculated and experimental spectra for $(SiH_3)_2O$ are compared in Figure 4, and indicate that the B3LYP/6-311N++G(3df,3pd) level of theory is able to capture most of the principal quantitative features observed. In particular we note that the intensity ratio among the peaks is well reproduced in the low frequency region and that the splitting between the asymmetric/symmetric Si−H bands in the high-frequency regime is accounted for. Here we follow our previous work on Si−Ge hydride molecules and apply low- and high-frequency scale factors of 0.989 and 0.979, respectively, to the calculated

Table 3. Thermochemical Data for the $(SiH_3)_2O$, $(GeH_3)_2O$, and $(GeH_3)O(SiH_3)$ Molecules[a]

molecule	E_0+H_{CORR}	E_0+G_{CORR}	ΔH_f^0	ΔH_f^0(*corrected*)
$(SiH_3)_2O$	−656.903268	−656.940769	−87.528	−83.127 **(−79.4 ± 2.0)**
$(GeH_3)_2O$	−4230.167739	−4230.207336	−40.998	−20.994
average	*−2443.535504*	*−2443.574053*	*−64.263*	*−52.061*
$(SiH_3)O$-(GeH_3)	−2443.536079	−2443.576044	−64.624	−52.422

[a] The first two columns list the enthalpy and free-energy corrected electronic energies (in Hartree units) while the third and fourth columns lists the standard and "corrected" heat of formation (in kcal/mol) for the compounds. (Note: 0.0368 H = 23.06 kcal/mol).

spectra. In the case of $(GeH_3)_2O$, our calculated spectrum agrees very well with the infrared spectrum and mode assignments reported previously by Cradock.[42] Although a numerical spectrum is not available, the most intense mode frequencies can be compared directly with the frequency-scaled theoretical values as follows (observed values in parentheses and cm^{-1}): G_0, 448 (452); G_2, 668(674); G_3, 787 (784/798); G_7, 883 (882); G_8, 919 (928/937); G_{10}, 2082 (2084); G_{12}, 2112 (2120).

3.4. Molecular Thermochemistry. In addition to providing total electronic energies and the equilibrium molecular structures, the Gaussian03 code was also used to generate enthalpy and free energy estimates at 298 K ($E_0 + H_{CORR}$ and $E_0 + G_{CORR}$, respectively). Using this data and the corresponding values for the atomic species, we computed the standard heat of formation ΔH_f^0 of $(SiH_3)_2O$, $(GeH_3)_2O$, SiH_3OGeH_3 using the formula

$$\Delta H^o_{f,298}(\mathrm{M}) = E(\mathrm{M}) + ZPVE(\mathrm{M}) + [H_{298}(\mathrm{M}) - H_0(\mathrm{M})] - \sum_{\mathrm{A}}^{atoms}\{E(\mathrm{A}) + [H_{298}(\mathrm{A}) - H_0(\mathrm{A})]\} + \sum_{\mathrm{A}}^{atoms}\Delta H^o_{f,298}(\mathrm{A}) \qquad (6)$$

where the energy difference between the molecule (M) and its constituent atoms (A) is offset by the experimental reference state, for example, the sum of atomic formation energies $\Delta H^0_{f,298}$ (the latter were obtained from the CODATA thermodynamic database[43]). The largest errors in this formula arise primarily from the treatment of exchange and correlation effects in the electronic energy. Thus, DFT-based methods involving local density or generalized gradient approximations (LDA and GGA) are not expected to be as accurate as the compound CBS-QB3 method which includes a non-local correlation treatment at the MP2 level. To improve the prediction of ground state thermochemical properties we determine a set of consistent atomic enthalpy corrections ξ_i for the H, O, Si, and Ge atoms using an optimization procedure which minimizes the deviations between experimental and calculated heats of formation for a large set of Si−Ge−O−H containing molecules.[44]

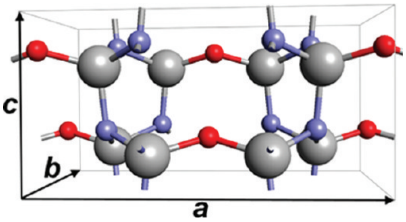

Figure 5. Prototype M_2N_2O orthorhombic unit cell showing the "layering" of the 8 M group IV sites (gray spheres). Note that the oxygen atoms (red) link these sites along the layers, while nitrogen atoms (blue) connect group IV sites between layers. Crystallographic axes are labeled by arrows.

Denoting the difference between the uncorrected enthalpy in eq 6 and the corresponding observed value by ΔH_0, and the stoichiometry numbers for each of the n elements in a given molecule by η_i, the minimization of $\Delta H(\vec{\xi}) = \Delta H_0 + \sum_{i=1}^{n}\eta_i\xi_i$ yields optimal atomic enthalpy corrections ξ_H = 0.565, ξ_O = 0.294, ξ_{Si} = 0.358, and ξ_{Ge} = 8.163 kcal/mol. These parameters represent a global minimum over the test set hydride molecules used as input, and are found to be insensitive to the initial conditions in the optimization procedure.

The corrected heats of formation obtained by this procedure are listed in Table 3 which indicates that $\Delta H^0_{f,298}$ is controlled by the strength of the M−O bonds, attaining the largest (−83.13 kcal/mol) and smallest (−20.99 kcal/mol) values in $(SiH_3)_2O$ and $(GeH_3)_2O$, respectively. As expected, the heat of formation −52.42 kcal/mol of $(GeH_3)O(SiH_3)$ is calculated to be intermediate to the values for $(SiH_3)_2O$ and $(GeH_3)_2O$, and close to their average of −52.06 kcal/mol indicating an *ideal additivitiy* behavior for Si−O and Ge−O bond enthalpies These trends are consistent with both the observed high thermal stability of $(SiH_3)_2O$ and the newly synthesized $(GeH_3)_2(SiH_2)_2O$ species,[41] and the relative instability of $(GeH_3)_2O$ which typically decomposes at room temperature to produce germane and H−Ge−O polymers. We note that our calculated value for the $(SiH_3)_2O$ enthalpy of formation (−83.1 kcal/mol) is very close to the experimentally determined value (−79.4 kcal/mol)[13]. The delicate energy balance between the SiH_3OGeH_3 species and the average of $(SiH_3)_2O$ and $(GeH_3)_2O$, expected on the basis of bond conservation, is also directly reflected in the free-energy corrected ground state electronic energies $E_0 + G_{CORR}$, whose difference is ~1.25 kcal/mol for these species.

4. Properties of Solid State Si_2N_2O, Ge_2N_2O, and $SiGeN_2O$

As discussed in the introduction pseudobinary intermediates between Si_2N_2O and Ge_2N_2O phases such as $(Si,Ge)_2N_2O$ or solid solutions with compositions $Si_{1-x}Ge_xN_2O$ may be of significant technological interest. A broad range of alloy polytypes can be envisioned on the basis of the simple orthorhombic Si_2N_2O prototype structure shown in Figure 5. The latter contains 8 group IV atom sites (gray spheres in Figure 5) which can be occupied in a variety ways to form highly ordered structures with four Si sites and four Ge sites (e.g., $SiGeN_2O$). When viewed along a direction normal to the b-axis these Si/Ge sites can be identified by

---

(42) Cradock, S. *J. Chem. Soc. A* **1968**, 1426.

(43) Cox, J. D.; Wagman, D. D.; Medvedev, V. A. *CODATA Key Values for Thermodynamics*; Hemisphere Publishing Corp.: New York, 1989; see also http://www.codata.org/resources/databases/key1.html.

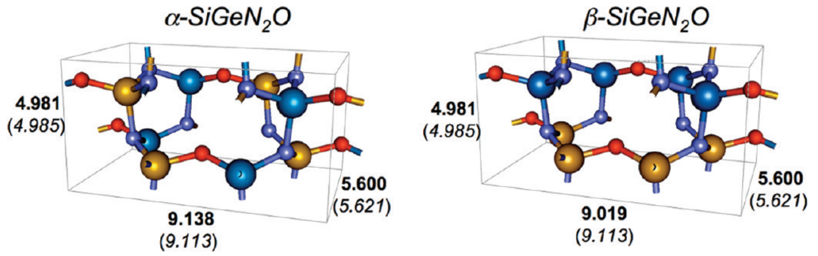

Figure 6. Calculated orthorhombic (Z = 4) cell parameters (bold font) of the α-SiGeN$_2$O and β-SiGeN$_2$O. Values in parentheses represent the average of the Si$_2$N$_2$O and Ge$_2$N$_2$O parameters and indicate a virtually ideal Vegard-like behavior. The crystallographic orientation is the same as in Figure 5.

Table 4. Optimized GGA (PW91) Structural Parameters and Energies of the Solid Phases Si$_2$N$_2$O, Ge$_2$N$_2$O, α-SiGeN$_2$O, and β-SiGeN$_2$O[a]

system	primitive cell parameters				atomic positions		pseudo-ortlwrhombic cell dimensions		
					Si$_2$N$_2$O				
	a (Å)	5.223	α (deg)	90	Si (8b):	(0.5222,0.1714,0.2913)	(α = β = γ = 90)		
$Cmc2_1$ (Z = 2)	b (Å)	5.223	β (deg)	90	N (8b):	(0.4114,0.8396,0.1399)	8.894	5.477	4.845
ρ(g/cm^3) = 2.820	c (Å)	4.845	γ (deg)	116.750	O (4a):	(0.2762,0.2762,0.2316)	***8.866***	***5.486***	***4.845***
Ω_0(Å^3) = 59.00									
E_0(H) = −1.50184									
					Ge$_2$N$_2$O				
	a (Å)	5.484	α (deg)	90	Ge (8b):	(0.5169,0.1697,0.2959)	(α = β = γ = 90)		
$Cmc2_1$ (Z = 2)	b (Å)	5.484	β (deg)	90	N (8b):	(0.4271,0.8339,0.1481)	9.331	5.764	5.125
ρ(g/cm^3) = 4.559	c (Å)	5.125	γ (deg)	116.591	O (4a):	(0.2469, 0.2469, 0.2055)	***9.317***	***5.752***	***5.105***
Ω_0(Å^3) = 68.91									
E_0(H) = −1.22774									
					α-SiGeN$_2$O				
	a (Å)	9.138	α (deg)	90	Si (2a):	(0.8341, 0.8145, 0.6847)	(α = β = 90, γ = 90.047)		
$P2_1$ (Z = 2)	b (Å)	4.981	β (deg)	31.506	Ge (2a):	(0.4801, 0.8160, 0.6961)	9.138	5.600	4.981
ρ(g/cm^3) = 3.769	c (Å)	5.359	γ (deg)	90	N (2a):	(0.8463,0.1546,0.7288)			
Ω_0(Å^3) = 63.74					N (2a):	(0.4130,0.1752,0.7612)			
E_0(H) = −1.36387					O (2a):	(0.7517,0.7437,0.5157)			
					β-SiGeN$_2$O				
	a (Å)	5.339	α (deg)	90	Si (4b):	(0.5113,0.1668,0.3058)	(α = β = γ = 90)		
Cm (Z = 2)	b (Å)	5.339	β (deg)	90	Ge (4b):	(0.4731,0.8257,0.8170)	9.091	5.600	4.981
ρ(g/cm^3) = 3.790	c (Å)	4.981	γ (deg)	116.731	N (4b):	(0.5536,0.1605,0.6471)			
Ω_0(Å^3) = 63.4O					N (4b):	(0.3878,0.8337,0.1741)			
E_0(H) = −1.36326					O (2a):	(0.2948, 0.2948, 0.2230)			
					O (2a):	(0.7734, 0.7734, 0.7570)			

[a] Lattice parameters and atomic positions are listed for primitive (Z = 2) unit cells. Volume (V in Å^3) and ground state electronic energy (E_0 in Hartree) are per formula unit, and equivalent pseudo-orthorhombic cell parameters are provided in the last column with experimental values where available. Experimental data (bold italic) for Si$_2$N$_2$O and Ge$_2$N$_2$O are taken from refs 45. and 46, respectively. (Note: 1 hartree = 627.51 kcal/mol).

their stacking sequence along the c-direction (we note that no oxygen linkages occur in this direction). We thus consider two simple choices: the first contains mixed Si−Ge occupancies within each layer and is designated α-SiGeN$_2$O, while a second choice, β-SiGeN$_2$O, is crafted by placing Si and Ge exclusively in alternating layers. In the following sections we consider in detail the crystalline properties of these two simple polytypes in relation to their parent phases Si$_2$N$_2$O and Ge$_2$N$_2$O, as shown in the simulated ground state unit cells shown in Figure 6 (see also Figure 9, below).

The VASP code was used exclusively to obtain the equilibrium crystalline, electronic and vibrational properties of the Si−Ge oxynitrides considered in the present study. In all calculations we adopted the PAW-GGA methodology based on the Perdew−Wang parametrization[32] of the exchange-correlation energy. For N, O, and Si atoms we employed the standard pseudopotentials to represent the s- and p- valence states, while 3d orbitals were also included in the case of Ge atoms. The optimization of the Si$_2$N$_2$O and Ge$_2$N$_2$O structures was carried out in a 10-atom (Z = 2) primitive unit cell setting (space group $Cmc2_1$), by simultaneously minimizing the atomic forces and the stress on the cells. We used an 800 eV energy cutoff for the plane-wave expansion and 80 irreducible k-points for Brillouin zone integrations to obtain highly converged structures with forces less than 0.0002 eV/Å and a residual external stress less than 0.01 kbar. For the α-SiGeN$_2$O and β-SiGeN$_2$O polytypes the 10-atom (Z=2) primitive representations possess a lower monoclinic/triclinic symmetry (space group $P2_1$ and Cm, respectively), and accordingly, a denser reciprocal space grid containing 150/300 irreducible k-points, respectively, was needed to generate the same quality of convergence as obtained for higher symmetry Si$_2$N$_2$O and Ge$_2$N$_2$O structures.

4.1. Crystal and Electronic Structure. The optimized lattice parameters of Si$_2$N$_2$O, Ge$_2$N$_2$O, α-SiGeN$_2$O, and β-SiGeN$_2$O are listed in Table 4, and indicate a very good agreement with the available experimental data. It should be noted that the latter compounds are typically obtained from powder data of polycrystalline samples. The slight overestimate seen in the theoretical predictions is a

Table 5. Average Bond Lengths and Bond Angles in Si_2N_2O, Ge_2N_2O, α-$SiGeN_2O$, and β-$SiGeN_2O$

Bond Lengths

	Si−O	Ge−O	Si−N	Ge−N
Si_2N_2O	1.633		1.728 ± 0.002	
Ge_2N_2O		1.774		1.840 ± 0.005
α-$SiGeN_2O$	1.635	1.770	1.731 ± 0.011	1.832 ± 0.005
β-$SiGeN_2O$	1.638	1.772	1.720 ± 0.004	1.846 ± 0.006

Bond Angles

	Si−O−Si	Ge−O−Ge	Si−O−Ge
Si_2N_2O	145.6		
Ge_2N_2O		131.9	
α-$SiGeN_2O$			138.3
β-$SiGeN_2O$	145.8	129.5	
	Si−N−Si	**Ge−N−Ge**	**Si−N−Ge**
Si_2N_2O	119.5 ± 4.0		
Ge_2N_2O		118.4 ± 3.2	
α-$SiGeN_2O$	120.5	114.2	118.1 ± 1.7
β-$SiGeN_2O$	131.2	114.1	114.0 ± 11.8
	N−Si−N	**N−Ge−N**	
Si_2N_2O	109.2 ± 2.2		
Ge_2N_2O		109.7 ± 1.8	
α-$SiGeN_2O$	109.7 ± 3.1	109.7 ± 1.0	
β-$SiGeN_2O$	109.7 ± 2.6	108.9 ± 3.0	

well-known artifact of the GGA implementation of DFT, which typically yields bond lengths 1−2% larger than those observed. However, in this case it appears to be well within the experimental uncertainty of the measurements (~0.5%). Our calculated structural data is also quite consistent with values obtained in earlier theoretical studies.[22,25,27] The structural parameters of the hypothetical α-$SiGeN_2O$ and β-$SiGeN_2O$ polytypes are predicted to be virtually identical. We note that the molar volume of the β-polymorph is found to be slightly lower than that of its α- counterpart, which may be associated with the slightly different packing obtained upon layering the SiN_3O and GeN_2O polyhedral units. As shown in Figure 6, the lattice parameters of α-$SiGeN_2O$ and β-$SiGeN_2O$ closely correspond to the Vegard average of Si_2N_2O and Ge_2N_2O (< 0.5% difference). The figure also shows the distribution of Si and Ge in the α- and β-polytypes.

The bond lengths and bond angles corresponding to the optimized structures are listed in Table 5. As can be seen from the data, the values for the Si−O and Ge−O bond lengths are remarkably consistent throughout the four compounds with small variations on the order of 0.005 and 0.002 Å, respectively. Similar consistency but slightly larger variations (~0.01 Å) are observed in the corresponding Si−N and Ge−N bonds, which exhibit a distribution in all structures. This is indicated by the ± values in the table, which represent departures from the mean values (both for bond lengths, and later in the table for bond angles). In the case of the α-$SiGeN_2O$ and β-$SiGeN_2O$ structures it is noteworthy that all bond lengths (with the exception of Si−N bonds) in the β-phase are slightly dilated with respect to those in the α-structure. The Si−O−Si and Ge−O−Ge bond angles are also essentially transferable (to within ~1°) between all structures, while the Si−O−Ge bond angle (138.3°) is virtually identical to the average (138.8°) of the Si−O−Si and Ge−O−Ge bond angles in Si_2N_2O and Ge_2N_2O, respectively. Perhaps not surprisingly, the same trend was noted at the molecular level (see Table 1) where the Si−O−Ge bond angle in SiH_3OGeH_3 (131°) was found to be only a few degrees smaller than the average of the M−O−M bonds in $(SiH_3)_2O$ and $(GeH_3)_2O$. Finally, we note that the largest angular deviations are found in the N−M−N tetrahedral and Si−N−Ge bonding distributions of the hybrid structures for which $\Delta\theta \sim 3°$ and ~12°, respectively. Such large deviations in bond angle are likely needed to compensate for the remarkable lack of bond strain, as evidenced by the consistency of Si−O, Ge−O, Si−N, and Ge−N bond lengths throughout all of the predicted ground state structures.

Figure 7 shows band structure plots for Si_2N_2O, Ge_2N_2O, α-$SiGeN_2O$, and β-$SiGeN_2O$, along with the corresponding density of states (DOS). As expected α-$SiGeN_2O$ and β-$SiGeN_2O$ exhibit electronic properties intermediate to those of Si_2N_2O and Ge_2N_2O. We used a common orthorhombic unit cell setting to map the band along a common *k*-space path to facilitate comparison between these systems. In the case of the slightly "pseudo-orthorhombic" α-$SiGeN_2O$ primitive cell, the structure was recast into a perfectly orthorhombic setting by adjusting the non-orthogonal *c*-axis (~0.05 degrees) to a right angle to simplify the comparison with the other systems. We have verified that the energy change associated with this orthorhombic symmetry constraint in α-$SiGeN_2O$ leads to very small (~ 0.1 meV/atom) increase in the total energy. However, note that the total energy data listed in Table 4 was calculated using the ground state primitive cells for all systems.

The band structure of the prototypical Si_2N_2O system has been previously[4,24,25] studied using DFT-LDA methods using a variety of methodologies including full potential linearized muffin-tin (FLMTO) and the orthogonalized linear combination of atomic orbitals (OLCAO), resulting in some ambiguity in the quantatitve outcome at the same level of theory. The most striking discrepancies involve the band widths and band gaps (E_g). In the latter case the values of the direct gap for Si_2N_2O range from 3.2 to 5.3 eV, while an *indirect* gap of ~6.0 eV has also been reported.[24] Corresponding direct energy gaps in Ge_2N_2O have been predicted in the range 2.0−3.8 eV. All of these values differ significantly from the experimental values of $E_g[Si_2N_2O] \sim 5.2-5.6$ eV (to our knowledge a reliable value for the band gap of Ge_2N_2O has yet to be determined). This level of uncertainty, both in the magnitude and character (direct/indirect) of the band gaps prompted us to carry out a series of state-of-the-art calculations using an efficient modern band structure approach, as implemented in the VASP code. All-electron-like PAW pseudopotentials generated at the GGA level were employed in all of our calculations. We adopted the same computational conditions as for the structure optimization

---

(44) Weng, C.; Chizmeshya, A.V.G. Thermodynamic Properties of Si-Ge Hydrides and their Chlorinated Analogs: Accurate Formation Enthalpies from First Principles. *J. Comp. Chem.*; submitted for publication.

(45) Idrestedt, I.; Brosset, C. *Acta Chem. Scand.* **1964**, *18*, 1879.

(46) Labbe, J. C.; M. Billy, C. R. *Acad. Sci. Ser. C* **1973**, *277*, 1137.

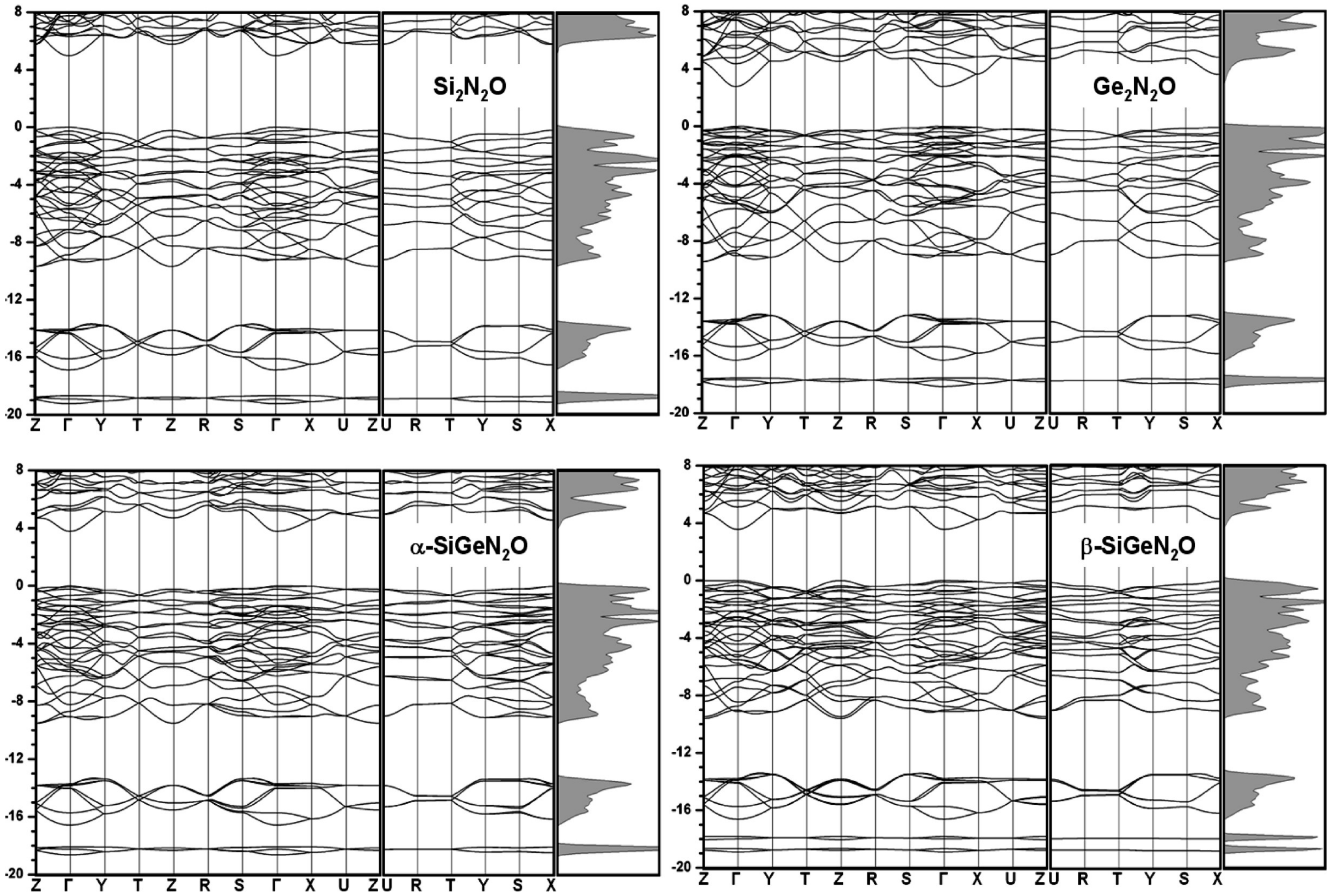

Figure 7. Band structure plots for Si_2N_2O, Ge_2N_2O, α-$SiGeN_2O$, and β-$SiGeN_2O$. The *k*-space path shown along the bottom of each plot corresponds to a common orthorhombic unit cell setting, and the vertical axis represents eigenvalues in eV (note that 1 eV = 23.06 kcal/mol). In the case of the α-$SiGeN_2O$ the slightly non-orthogonal *c*-axis (~0.05 degrees) was set to a right angle for the purpose of the band-structure comparison.

Table 6. Table of Calculated E_g Indicating That All Compounds Exhibit Direct Band Gaps in the Range 3.5−4.9 eV[a]

system	E_g (eV)	VB→CB (character)
Si_2N_2O	4.86	Γ (d,p) → Γ (p,s)
Ge_2N_2O	2.72	Γ (d,p) → Γ (s)
average	3.79	
α-$SiGeN_2O$	3.69	Γ (d,p) → Γ (s)
β-$SiGeN_2O$	3.53	Γ (d,p) → Γ (s)

[a] The corresponding nature and location (in *k*-space) of the CB and VB states is indicated in the third column.

described above; however, the *k*-point integrations used in the final density and SCF Kohn−Sham potential were carried out using a more accurate "tetrahedron method". The resulting band structure for the Si_2N_2O system is shown in the top left panel of Figure 7.

The origin of the bands was analyzed by examining the contributions from s, p, and d angular momentum projections of the various bands for Si, Ge, N, and O. In general we find that the conduction band (CB), valence band (VB), and semi-localized states below −10 eV all have a common origin with regards to the hybridization among the constituent atoms. Specifically, in all cases the valence band originates predominantly from mixing of O and N p-orbitals. The outer Si and Ge occupied p-orbitals also contribute near the center of the VB, while their corresponding s-states are dominant in the bottom 2 eV portion. For both of these features the Ge atom makes a stronger contribution than its Si counterpart.

In all compounds the conduction band devolves mainly from a mixture of unoccupied Si/Ge s- and p-states, and their hybridization with a lesser p-state contribution from nitrogen. We note that in Si_2N_2O the CB edge possesses p-character, while in all other compounds the unoccupied 4s states of Ge dominate this energy range. Finally, all compounds are found to exhibit DFT-GGA direct gaps in the range 2.72−4.86 eV, as shown in Table 6. In all cases the band character of the relevant VB and CB edge states is expected to lead to direct transitions, as indicated by the designations in parentheses, which list the dominant character as the first entry followed by the minor one. While these values are consistent with those calculated in earlier work,[4,24,25] they were all obtained using a consistent methodology for the first time. This is necessary to establish reliable trends across this family of compounds. Our data shows that the $SiGeN_2O$ compounds exhibit band gaps close to a Vegard average with a slight negative bowing of 0.1−0.3 eV, and that the difference between the gaps of the α- and β-polytypes is about 0.2 eV, with the α-$SiGeN_2O$ gap (~ 3.7 eV) being closest to the average (3.8 eV).

The remaining set of bands occurring directly below the main VB (e.g., < −10 eV) possess primarily N(2s) character, with a minor Si or Ge atom p-orbital contribution. These bands appear to be quite independent of the chemical composition, as evidenced by the robust and immutable structure of the DOS feature between −14 and −17 eV. Finally, below this latter manifold of states lies a much narrower, semilocal band of purely oxygen-2s origin which occurs near −18 eV in Si_2N_2O and −19 eV in Ge_2N_2O. In the α-$SiGeN_2O$ polytype this band occurs at an intermediate energy of −18.5 eV, as might be expected since the oxygens occur exclusively in Si−O−Ge units. By contrast, both the −18 eV and −19 eV bands remain distinct in the anisotropic β-$SiGeN_2O$ compound, which is consistent with a lamellar structure in which the Si- and Ge-layers contribute independently to the band structure. Accordingly, this narrow band may serve as an excellent spectroscopic feature to distinguish the various Si−Ge oxynitride polytypes.

4.2. Compression Equations of State. The incorporation of strong Si−N bonds (trigonal nitrogen) and tetrahedrally coordinated silicon in Si_2N_2O imbues the material with thermoelastic properties intermediate to those of its structuro-chemical Si_3N_4 and SiO_2 components. Prior theoretical work has demonstrated that this is a useful analogy for elucidating the origin of the electronic structure and optical properties of Si_2N_2O.[4] In the case of its bulk modulus, B_0, a comparison with Si_3N_4 ($B_0 \sim 230$ GPa) and SiO_2 ($B_0 \sim 30$ GPa) suggests that $B_0[Si_2N_2O] \sim 130$ GPa. A similar calculation for the Ge analogue using Ge_3N_4 ($B_0 \sim 160$ GPa) and GeO_2 ($B_0 \sim 30$ GPa) yields an estimate of ∼95 GPa for $B_0[Ge_2N_2O]$. Recent high-pressure hydrostatic compression experiments on Si_2N_2O corroborate this expectation and report a bulk modulus near 127 GPa,[22] while previous first-principles calculations based on LDA and/or GGA have produced values ranging from 130 to 180 GPa. In view of this latter variability in theoretical values for Si_2N_2O, and since experimental compression data for Ge_2N_2O is limited (see below), it is of considerable interest to pursue a systematic study of the compression behavior Si−Ge−O−N compounds. The pressure dependence of the enthalpy *difference* between the $SiGeN_2O$ polytypes and the Vegard average of Si_2N_2O and Ge_2N_2O, is also of interest since it provides additional information about the stability of these new materials at high pressure.

A common computational approach for obtaining the compression equation of state (EOS) of a solid is to calculate its relaxed crystal structure at a series of fixed volumes, by allowing the internal coordinates and "shape" of the unit cell to vary. The resulting energy-volume data is then typically fitted to a third order Birch−Murnaghan[35] $E(V)$ form to obtain the equilibrium energy (E_0), volume (V_0), B_0, and bulk modulus derivative at $P = 0$ (B_0'). Here we adopt an alternative "finite stress" approach in which the enthalpy, $H(P) = \min_V[E(V) + PV]$, is directly minimized at a series of fixed pressures (P) by varying the internal coordinates and cell parameters. We note that all such structure optimizations are carried out without imposing symmetry constraints (e.g., using $P1$ symmetry). The energy−volume data obtained from this procedure is then also fitted to a third order Birch−Murnaghan (B-M) EOS to obtain the parameters E_0, V_0, B_0, and B_0'. As an internal consistency check, the latter EOS was differentiated analytically to verify that the pressures corresponding to each data point match the input pressures employed in the finite stress calculations. Using the convergence conditions and structural tolerances described above (Section 4 introduction) we find that the deviation between the fit-derived pressures and those used as input is 1−2% over the range of pressures from −10 to 25 GPa used in our study.

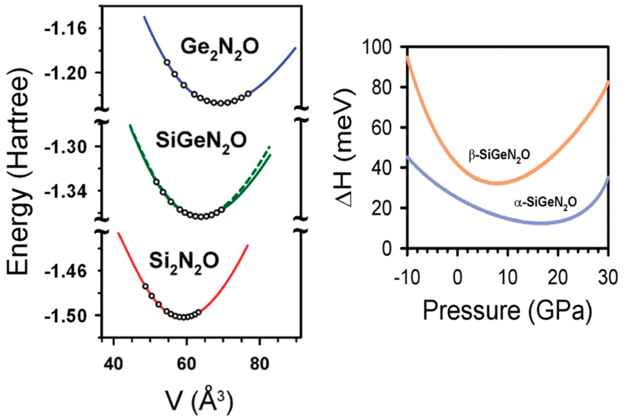

Figure 8. Left panel: Calculated compression equations of state data (circles) for Si_2N_2O, Ge_2N_2O, α-$SiGeN_2O$, and β-$SiGeN_2O$. The corresponding Birch−Murnaghan fits are ploted as solid red, blue, green, and green-dashed lines, respectively. Right panel: Static enthalpy differences between the α-$SiGeN_2O$ and β-$SiGeN_2O$ phases and the average enthalpy of Si_2N_2O and Ge_2N_2O indicating a minimum metastability the α- and β- structures at ∼17 and ∼8 GPa, respectively. (Note: 1 hartree = 627.51 kcal/mol, and 1 meV = 0.023 kcal/mol).

Table 7. Calculated Compression Equation of State Parameters of Si_2N_2O, Ge_2N_2O, α-$SiGeN_2O$, and β-$SiGeN_2O$, Indicating That the Proposed Hybrid Structures Exhibit Properties Very Close to the "Vegard Average" of the Corresponding Si_2N_2O and Ge_2N_2O

	E_0 (H)	V_0 (Å^3)	B_0 (GPa)	B_0'
Si_2N_2O	−1.50184	58.995	129.1	0.532
Ge_2N_2O	−1.22774	68.912	91.0	1.529
Vegard average	*−1.36497*	*63.954*	*110.1*	*1.03*
α-$SiGeN_2O$	−1.36387	63.723	107.5	1.254
β-$SiGeN_2O$	−1.36326	63.535	117.7	0.919

The results of our compression EOS calculations for Si_2N_2O, Ge_2N_2O, α-$SiGeN_2O$, and β-$SiGeN_2O$ are presented in Figure 8, and indicate that the energy−volume data (circles) is very well represented by the analytic Birch−Murnaghan EOS form (solid and dashed lines). The binding energy trend is clearly evident from the plots (Si_2N_2O > $SiGeN_2O$ > Ge_2N_2O) which also indicate decreasing compressibility in going from Ge_2N_2O to Si_2N_2O. The EOS parameters for all four solids, obtained from our best fit to the B-M equation of state, are listed in Table 7. Our calculated value for the bulk modulus of Si_2N_2O, 129 GPa, is quite close to the value 130 GPa reported recently by Kroll[19] using an almost identical and high-quality computational procedure. Both of these values closely match the experimental value of 127 GPa obtained via neutron diffraction at low-pressures ($P < 3$ GPa), and somewhat overestimate the value of 115 GPa recently obtained by Haines et al.[22] using an extended compression range ($P < 50$ GPa). The latter authors also

Table 8. Ground State Electronic Energy (E_0), Atomization Energy (E_A), and Vibrational Free Energy Correction ΔG(300 K) per Formula Unit (in Hartree) for the Si_2N_2O, Ge_2N_2O, α-$SiGeN_2O$, and β-$SiGeN_2O$ Solid Phases[a]

system	methodology	E_0	E_A	ΔG(300 K)
Si_2N_2O	VASP (PW91)	−1.50184	−1.17048	0.01293
Ge_2N_2O	VASP (PW91)	−1.22774	−0.90402	0.02330
α-$SiGeN_2O$	VASP (PW91)	−1.36387	−1.03633	0.01958
β-$SiGeN_2O$	VASP (PW91)	−1.36326	−1.03572	0.01932

[a] Note: 1 hartree = 627.51 kcal/mol.

report an anomalously small value for the bulk modulus derivative $B_0' \sim 1.2$, which they ascribe to the possible effect of non-hydrostatic stress in their experiments. However, the corresponding bulk modulus derivative values for all of our simulated structures is also in this range ($B_0' \sim 0.5-1.5$), suggesting that this may be a characteristic value for these materials and not an experimental artifact. The compressibility of Ge_2N_2O has also been determined experimentally to be ~101 GPa,[26] which is somewhat higher than our theoretical value of 91 GPa. The origin of the discrepancy is likely related to inaccuracies associated with the severely limited compression range ($P < 3$ GPa) used in their experiment.[26]

Also listed in Table 7 are the "Vegard average" EOS parameters of Si_2N_2O and Ge_2N_2O, which correspond closely to those of α-$SiGeN_2O$ and β-$SiGeN_2O$. We note, however, that while the energy and volume of the α- and β- are very similar, the bulk modulus of β-$SiGeN_2O$ (118 GPa) is ~9.5% larger than that of the α−$SiGeN_2O$ phase (108 GPa). This increase might be explained by the presence of the more rigid biaxial Si-bonded layers in β-$SiGeN_2O$. Nevertheless, the average of the α- and β- bulk moduli (113 GPa) is close to the Vegard average of the Si_2N_2O and Ge_2N_2O values (110 GPa). The compression mechanism in all of the four solids considered above was elucidated by examining the structural data in our models (e.g., the M−(N/O) bond lengths and M−O−M′ bond angles) as a function of pressure. Over the pressure range −10 to 25 GPa the volume change in all four compounds is found to be directly correlated with the tilting of the SiN_3O/GeN_3O tetrahedra, as suggested by the prior experimental studies of Srinisvasa and co-workers.[26]

Finally, we note from the static lattice equilibrium (electronic) energies in Table 7 that the α-$SiGeN_2O$ and β-$SiGeN_2O$ phases are marginally metastable with respect to an equivalent stoichiometric mixture of Si_2N_2O and Ge_2N_2O. Using the EOS fit data it is trivial to construct the enthalpy functions for the relevant phases to examine the phase stability of the α- and β- polytypes as a function of pressure. The enthalpy difference functions are plotted in Figure 8 in meV per formula unit, and indicate that α-$SiGeN_2O$ and β-$SiGeN_2O$ achieve metastability minima with respect to the Si_2N_2O/Ge_2N_2O mixture at ~17 GPa and ~8 GPa, respectively. The small energy differences, particularly for the α-$SiGeN_2O$ phase, suggest that these compounds might even be accessible via high pressure. However, important mixing entropy contributions and thermal corrections may alter the quantitative estimation of the critical pressures.

5. Formation of Si_2N_2O, Ge_2N_2O, and $SiGeN_2O$ from Molecular $MH_3OM'H_3$ (M, M′ = Si, Ge) Building Blocks

5.1. Reaction Thermodynamics. The calculated ground state energies and thermochemistry of the gaseous and solid reactants/products provided in Tables 1 and 8, respectively, can be used to estimate the standard free energies of reaction, ΔG_f^θ, for reactions involving the $(MH_3)O(M'H_3)$ precursors {M,M′ = Si, Ge} in a large excess of ammonia to yield the Si_2N_2O, Ge_2N_2O, α-$SiGeN_2O$, and β-$SiGeN_2O$ solid products and an H_2 byproduct (see eqs 7−10 below). One of the key contributions to the reaction thermodynamics is the electronic energy, which reflects the changes in bonding between reactants and products. According to our tabulated results (Tables 1 and 8) the electronic energies of both gaseous and solid species are most systematically reproduced by the DFT treatment based on the Perdew−Wang (PW91) parametrization of the GGA, as implemented by the VASP code. Accordingly, our calculations here combine the VASP(PW91) electronic energies for the gaseous and solid species with the free energy corrections at $T = 300$K, listed as ΔG(300 K). For the molecules, the latter correction includes translational, rotational and vibrational contributions, as well as the term $\Delta N RT \sim \Delta P V$, which accounts for possible molar changes in gas phase constituents in the reactions. In the case of solids the VASP(PW91) electronic energy is combined with a quasi-harmonic approximation of the vibrational free energy eq 5 to provide an estimate of the Gibbs free energy, which is computationally consistent with the molecular treatment. Using the data provided in Tables 1 and 8, and the foregoing prescription, we obtain the following reaction thermodynamics:

$$SiH_3OSiH_3(g) + 2NH_3(g) \rightarrow Si_2N_2O(s) + 6H_2(g) \quad (7)$$

$$\Delta E_0(1) = -56.1 \text{ kcal/mol}$$
$$\Delta G_f^0(1) = -90.6 \text{ kcal/mol}$$

$$GeH_3OGeH_3(g) + 2NH_3(g) \rightarrow Ge_2N_2O(s) + 6H_2(g) \quad (8)$$

$$\Delta E_0(1) = +15.2 \text{ kcal/mol}$$
$$\Delta G_f^0(1) = -7.0 \text{ kcal/mol}$$

$$\frac{1}{2}SiH_3OSiH_3(g) + \frac{1}{2}GeH_3OGeH_3(g) + 2NH_3(g) \rightarrow \beta\text{-}SiGeN_2O(s) + 6H_2(g) \quad (9)$$

$$\Delta E_0(1) = -20.4 \text{ kcal/mol}$$
$$\Delta G_f^0(1) = -48.8 \text{ kcal/mol}$$

$$SiH_3OGeH_3(g) + 2NH_3(g) \rightarrow \alpha\text{-}SiGeN_2O(s) + 6H_2(g) \quad (10)$$

$$\Delta E_0(1) = -19.7 \text{ kcal/mol}$$
$$\Delta G_f^0(1) = -47.1 \text{ kcal/mol}$$

On the basis of the static electronic energies ΔE_0 alone, these results indicate that the energetic "driving force" for the

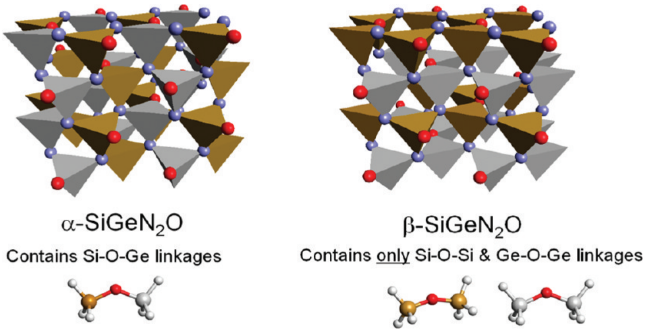

Figure 9. Hypothetical ordered solid phases of $SiGeN_2O$ containing solely Si−O−Ge units (α-$SiGeN_2O$), or an equal mixture of Si−O−Si and Ge−O−Ge building blocks (β-$SiGeN_2O$). Note that the latter structure possesses a lamellar stacking of purely $SiON_3$ and $GeON_3$ tetrahedral layers.

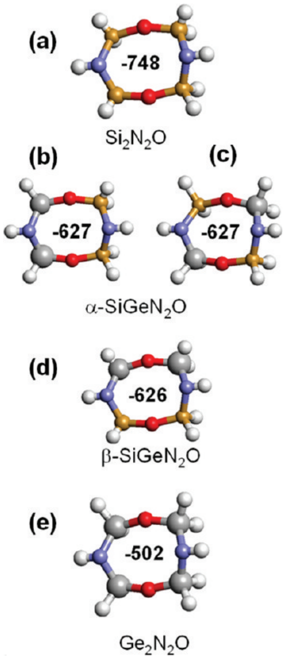

Figure 10. Molecular models of the four-member prototype clusters and their calculated formation energies from standard states (ΔE_f), given in kcal/mol per atom. Note that the latter decreases in proportion to the number of Ge−N bonds.

reaction 7 is considerably larger than that for reaction 8. The calculated values of $\Delta G_f^0(1)$ corroborate this trend and clearly indicate that reaction of $(SiH_3)_2O$ to form Si_2N_2O is expected to be most favorable from an experimental perspective. Nevertheless, we note that the corresponding reaction of $(GeH_3)_2O$ is calculated to be slightly exothermic (−7 kcal/mol), indicating that formation of Ge_2N_2O using this method is not as favorable.

The numerical average reaction energies 7 and 8 can be easily seen to yield $\Delta E_0(1+2)_{AVG} = -20.4$ kcal/mol and $\Delta G_f^0(1+2)_{AVG} = -48.8$ kcal/mol, respectively, suggesting that ammonia reacted with a mixture of $(SiH_3)_2O$ and $(GeH_3)_2O$ may provide a possible route (eq 9) to the lamellar-type β-$SiGeN_2O$ oxynitride solids composed of an equal mixture of Si−O−Si and Ge−O−Ge building blocks, as shown in Figure 9. Reaction 10 describes an alternative route to the $SiGeN_2O$ polytypes via reaction of ammonia with a single source precursor SiH_3OGeH_3 which implicitly includes Si−O−Ge building blocks, suitable for the formation of α-$SiGeN_2O$ (see Figure 9).

The ground state structures of the $SiGeN_2O$ polytypes, shown in Figure 9, clearly highlights the difference in network linkage with respect to the positions of both the nitrogen and the oxygen atoms, and the resulting stacking order of the $SiON_3$ and $GeON_3$ tetrahedra in both the α- and β- structures. While the α-$SiGeN_2O$ can be envisioned to form uniquely from the SiH_3OGeH_3 monomer, the synthesis of the β-$SiGeN_2O$ as described in reaction eq 9 does not take into account the competing reaction involving the individual $(SiH_3)_2O$ or $(GeH_3)_2O$ molecules with ammonia to form a mixture of Si_2N_2O and Ge_2N_2O oxynitrides, rather than the desired $SiGeN_2O$ phase. To elucidate the possible reaction pathway en route to the extended structures of the condensed phases, we examined the formation energy of prototype nanoscale building blocks obtained by linking the three oxygen-bridged precursor cores such as Si−O−Si, Ge−O−Ge, and Si−O−Ge. As shown in Figure 10 the latter are interconnected via trigonal nitrogen (as in the solids) to form eight-member rings inherent to the average structure of typical $SiO_2-Si_3N_4$ covalent networks. Accordingly, the stability of the α-$SiGeN_2O$ and β-$SiGeN_2O$ solid structures are expected to be closely related to the energetics of these elementary bonding arrangements. A basic account of the relative stability of such clusters was obtained by computing the electronic energy difference ΔE_0 between each ring structure and its corresponding "standard state" constituents as shown by the thermochemical reaction below, where (M,M′) = {Si,Ge}:

$$(MH_2)_2(M'H_2)_2O_2(NH)_2(g) \rightarrow 2M(s) + 2M'(s) + O_2(g) + N_2(g) + 5H_2(g) + \Delta E_0 \qquad (11)$$

The VASP DFT code was used to calculate the equilibrium structures and energies of the required solid and gas phase components in the above reaction. As for the gas phase calculations of the simpler molecules using VASP (described in Section 3), a slightly orthorhombic supercell with edge lengths ~20 Å was used to represent the isolated molecular species. We note that isolated atoms/molecules treated in a completely symmetric cell have a tendency to converge to a false minimum; thus, a slightly distorted cell is used to reduce the symmetry. The PAW-GGA methodology was employed with an 800 eV energy cutoff for the plane-wave expansion, and a 10 × 10 × 10 Monkhorst-Pack k-point grid for the solid phases (a single k-point at Γ was used for the molecular calculations).

The formation energies obtained from this procedure are superimposed upon the structural models shown in Figure 10. The results show that the homonuclear $(GeH_2)_4O_2(NH)_2$ and $(SiH_2)_4O_2(NH)_2$ are, respectively, the most weakly and strongly bound structures, while the heteronuclear analogues $(SiH_2)_2(GeH_2)_2O_2(NH)_2$ possess a formation energy intermediate to the latter and close to their numerical average, as expected. Accordingly the formation energies in Figure 10 indicate that the competing reaction of $(GeH_3)_2O$ with ammonia *in the presence of* $(SiH_3)_2O$ might show a propensity to form

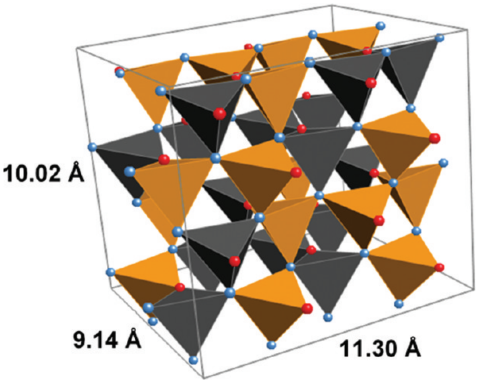

Figure 11. Representative 1 × 2 × 2 supercell model of a random $SiGeN_2O$ alloy showing distribution of $SiON_3$ (gold) and $GeON_3$ (gray) tetrahedra. Optimized lattice parameters (in Å) are indicated on the structure.

(d) rather than (e). The $(SiH_2)_2(GeH_2)_2O_2(NH)_2$ cluster would then combine with the dominant $(SiH_2)_4O_2(NH)_2$ species to produce silicon-rich alloys $Si_{2x}Ge_{2(1-x)}N_2O$ with $x > 0.5$ as described by reaction 12:

$$xSiH_3OSiH_3(g) + (1-x)GeH_3OGeH_3(g) + 2NH_3(g) \rightarrow Si_{2x}Ge_{2(1-x)}N_2O(s) + 6H_2(g) \quad (12)$$

$$\Delta G_f^0(3) = -91x - (1-x)7$$

Conversely, our calculations indicate that the intermediate structures such as (b) and (c), formed from the hybrid precursor SiH_3OGeH_3, are energetically very similar to the intermediate (d) suggesting that the most likely route to single phase α-$SiGeN_2O$ is that described by reaction eq 10.

As mentioned above in the context of pressure dependence of the enthalpy the lowering of the free-energy and enthalpy of $Si_{1-x}Ge_xN_2O$ phases via disordering of the Si/Ge sublattice may represent and important stabilization mechanism. From the data in Table 4 we find that the α- and β- polytypes of the $SiGeN_2O$ are metastable by 25.0 and 41.6 meV (per formula unit) relative to average of Si_2N_2O and Ge_2N_2O. Besides the vibrational energy corrections discussed in this section (see Table 8) there are no other configurational entropy contributions since both polytypes are ordered. On the other hand, our analysis of the bonding in the solid phases indicates that the M−O and M−N (M = {Si,Ge}) bonds are remarkably transferable among the tetrahedral units. Accordingly, we expect that the disordering of the Si/Ge sublattice will have a very small effect on the lattice enthalpy. To verify this expectation we have conducted calculations on a random $SiGeN_2O$ alloy (50% Si, 50% Ge) using a pseudocubic 1 × 2 × 2 supercell based on the structures shown in Figure 6. Using the same PAW-GGA prescription as above, and identical energy cutoffs but only 4 irreducible *k*-points, the structures were converged with residual forces of less than 0.0002 eV/Å and essentially zero cell stress. The representative structure in Figure 11 shows a possible quasi-random distribution of $SiON_3$ and $GeON_3$ tetrahedra. We note that the α- and β- structure were also optimized using the same procedure, and in the same supercells as a reference, yielding energies within a few dozen microHartree of the ones listed in Table 4. Averaging over three such random configurations yielded a mixing enthalpy estimate of 38.5 meV per formula unit (again relative to the average of Si_2N_2O and Ge_2N_2O). Using an ideal mixing assumption, the corresponding mixing entropy $-TS_{mix} \sim -17.9$ meV per formula unit for a 50% alloy, yielding a Gibbs free energy of approximately 20.6 meV at 300 K. This demonstrates that thermodynamic mixing provides only a slight stabilization in these systems with respect to the ordered α- and β- polytypes, and suggests that the latter are slightly higher in free-energy compared to their random counterpart by ~4 and 11 meV per formula unit, respectively. Accordingly, at room temperature both the α- and the β- structures are expected to be energetically competitive with a random alloy of the same stoichiometry. We note that for the latter $\Delta G_f = 0$ at $T \sim 560$ K indicating additional stabilization because of mixing entropy at higher temperatures, as expected. In view of the close similarity in the free-energies of the ordered and random phases it is likely that the reaction kinetics, associated with the different synthesis routes discussed above, will play a key role in the formation of the $SiGeN_2O$ solid.

6. Conclusions

We have presented a systematic simulation study of the thermochemistry involved in the formation of $Si_{1-x}Ge_xN_2O$ oxynitrides based on reactions of both $(SiH_3)_2O$ and $(GeH_3)_2O$ molecules, and the proposed SiH_3OGeH_3 analogue, in an ambient of ammonia. Our main conclusion is that a broad range of $Si_{1-x}Ge_xN_2O$ oxynitrides can be synthesized using this approach, depending on the proportions of $MH_3OM'H_3$ precursors used in the reactant mixture. Silicon-rich alloys $Si_{2x}Ge_{2(1-x)}N_2O$ with $x > 0.5$ are expected if a mixture of $(SiH_3)_2O$ and $(GeH_3)_2O$ molecules is reacted with ammonia. Two new ordered structures are proposed for the $SiGeN_2O$ composition: (i) an α-$SiGeN_2O$ phase composed of a uniform distribution of SiN_3O and GeN_3O tetrahedra, and a "pseudo-lamellar" form β-$SiGeN_2O$ in which the SiN_3O and GeN_3O units occupy alternating layers. Thermodynamic considerations suggest that while both of these ordered phases are expected to be slightly metastable under ambient conditions , the condensation of α-$SiGeN_2O$ is slightly favored, and a random $SiGeN_2O$ alloy analogue should possess a comparable enthalpy of formation. The latter result indicates that mixing entropy should stabilize the disordered solid at high temperatures. Cluster calculations on nanoscale rings endemic to the internal structure of the proposed $Si_{1-x}Ge_xN_2O$ phases suggest that the most facile route to α-$SiGeN_2O$ is through reactions of SiH_3OGeH_3 with ammonia.

Our work also provides guidance with regards to the expected properties of $(GeH_3)_2O$ and SiH_3OGeH_3, as well as those of the α-$SiGeN_2O$ and β-$SiGeN_2O$ polytypes. For both molecules and solids our simulations indicate that the energy differences between the heteronuclear molecules (and corresponding solids) differ only slightly from the stoichiometric combination of their homonuclear counterparts. In addition, we find a remarkably robust transferability of the M−O and M−N (M = {Si,Ge}) bond properties between/among the molecules and solids, leading to a striking observance of Vegard's law in many, if not all, of the associated properties.

The excellent agreement between the observed and calculated structural, vibrational and thermoelastic properties of the known compounds [$(SiH_3)_2O_{(g)}$, $(GeH_3)_2O_{(g)}$, $Si_2N_2O_{(s)}$] suggests that our predictions for the lesser known (or unknown) analogues may provide a useful guide for future experimental work in this class of materials. In particular, solid Si−Ge−O−N phases may be immediately relevant in the emerging area of high-*k* gate materials for use in next-generation high mobility Si−Ge based transistors.

Acknowledgment. The work was supported by AFOSR MURI (FA9550-06-01-0442), DOE (DE-FG36-08GO18003) and NSF Focused Research Group (DMR-0907600). Computational studies were performed using the resources of the Fulton High Performance Computing Initiative at Arizona State University. We would also like to thank an anonymous reviewer for several useful comments and suggestions.